< Electronic Supplementary Information >

Anisotropic Lens-shaped Mesoporous Carbon from Interfacially Perpendicular Self-Assembly for Potassium-Ion Battery

Dongyoon Woo,‡ Minkyeong Ban,‡ Jisung Lee, Cheol-Young Park, Jinuk Kim,

Seongseop Kim,* and Jinwoo Lee*

Chemicals

Homo-poly(methyl methacrylate) (hPMMA) (996 kg mol^{-1}), aluminum *sec*-butoxide ($Al(OBu^s)_3$), (3-glycidyloxypropyl-)trimethoxysilane (Glymo), poly(melamine-co-formaldehyde) (melamine–formaldehyde resin) (M_n = ~432 g mol^{-1}, 84 wt% in 1-butanol) were purchased from Sigma-Aldrich. Chloroform ($CHCl_3$), tetrahydrofuran (THF), and concentrated HCl (35−37%) were purchased from Samchun (Korea). Phenol-formaldehyde resin (PF resin) was prepared by previous reported method.[1] Poly(ethylene oxide)-*block*-poly(styrene) (PEO-*b*-PS) was prepared by atomic transfer radical polymerization (ATRP).

Experimental section

Synthesis of aluminosilicate sol (AS sol). 0.313 g of aluminum *sec*-butoxide, 2.703 of Glymo, and 0.011 g of KCl were mixed and 0.135 g of 0.01 M HCl was added dropwise in an ice bath. The mixture was stirred for 15 min at the ice bath, then stirred for another 15 min at room temperature. Then 0.765 g of 0.01 M HCl was added slowly for 10 min. After, stirring for 25 min, AS sol was obtained by filtration through a 0.2μm PTFE syringe filter to remove KCl.

Synthesis of lens-shaped nitrogen-doped mesoporous carbon (Lens-NMC). 1.4g of

hPMMA. 0.2g of PEO-b-PS and 0.7g of AS sol, and 0.14 g of carbon precursor (PF and MF resin, 1:1 w/w) were dissolved in 15ml THF and 25 ml $CHCl_3$. After 2 h stirring, transparent solution was poured into the petri dish. Solution was evaporated at 50°C and then hPMMA/PEO-b-PS/AS/carbon precursor hybrids were annealed at 100 °C for overnight. The as-made hybrids were re–dissolved in THF and centrifuged to remove hPMMA matrix. Centrifuged hybrids were calcined at 900°C for 2 h under inert condition with heating rated of 1 °C min^{-1}. To remove AS species, AS/N-doped carbon composite was immersed in HF solution (40-45% HF aqueous solution, DIW, and EtOH, 2:9:9 volume ratio) and washed with ethanol and distilled water and dried vacuum oven at 60°C over night.

Synthesis of lens-shaped mesoporous carbon (Lens-MC). Synthesis of Lens-MC was same with Lens-NMC except that only PF resin was dissolved in solvent as carbon precursor.

Synthesis of bulk mesoporous carbon (BMC). 0.15 g of PEO-b-PS and 0.164 g of RF resin were dissolved in 7ml of THF. 0.306ml of TEOS and 0.137 ml of 0.2M HCl were added to above solution dropwise. After stirring about 1 hour to get homogeneous solution, the mixture was poured into petri dish and evaporated at 50°C. After evaporation was finished, the film was further annealed at 100 °C for overnight. After annealing, the as-made film was carbonized at 900°C for 2 h under inert condition with heating rated of 1 °C min^{-1}. To remove silica, the carbonized product was etched by HF solution (40-45% HF aqueous solution, DIW, and EtOH, 2:9:9 volume ratio) and washed with ethanol and distilled water, then dried under vacuum oven at 60°C over night.

Material characterization. Gel permeation chromatography (GPC; Waters) was carried out using THF as the eluent. The nanostructure was characterized by transmission electron microscopy (TEM, H-7650, Hitachi) n the Center for University-wide Research Facilities

(CURF) at Jeonbuk National University and scanning electron microscopy (SEM, S-4700 field emission SEM, Hitachi) at the Future Energy Convergence Core Center (FECC). The powder X-ray diffraction (XRD) patterns were obtained on a Rigaku SmartLab using Cu Kα. X-ray photoelectron spectroscopy (XPS) was detected with ThermoFisher Scientific K-Alpha+. The nitrogen physisorption was analyzed at 77 K using Tristar II 3020 (Micromeritics Instrument Co.). The specific surface area was calculated by The Brunauer-Emmett-Teller (BET) method using adsorption data in a relative pressure range from 0 to 0.3. The pore size distribution was measured by the Horvath-Kawazoe method in the micropore region (< 2 nm) and the Barrett-Joyner-Halenda (BJH) method in the mesopore region (> 2 nm). Small angle X−ray scattering (SAXS) measurements were carried out on the 4C SAXS beamline at the Pohang Light Source II. Electroconductivity of manufactured carbon electrode was measured with 4-point probe method with CMT-100MP, AIT. Fourier transform infrared (FT-IR) spectroscopy was performed using a Thermo Fisher Scientific Nicolet iS50 instrument. The samples were prepared as pellets mixed with potassium bromide (KBr).

Electrochemical Characterization. For the half-cell test, K metal was used as the counter electrode, and Lens-NMC, Lens-MC, or BMC were used as the working electrode. BMC. To assess the performance of the half-cell, a configuration involving CR2032-type coin cells was employed., which were assembled in a glove box. A GF/F glass microfiber filter (Whatman, USA) was used as a separator. The electrolyte consisted of a 1 M potassium bis(fluorosulfonyl)imide (KFSI) dissolved in a 1:1 (v/v) mixture of ethylene carbonate (EC) and diethyl carbonate (DEC). The working electrode was prepared via typical slurry and casting methods. The slurry was formulated by blending 70 wt % Lens-NMC, Lens-MC or BMC, 20 wt % Super P, and 10 wt % poly(vinylidene fluoride) (PVDF) and then pasted on Cu

foil. The galvanostatic electrochemical test was conducted by a WBCS-3000 battery cycler (WonATech Co., Korea) in the potential range of 0.01 to 3 V (versus K/K^+). Electrochemical impedance spectroscopy was conducted utilizing the potentiostat (Reference 600, Gamry Instruments, USA) with an amplitude of 5 mV, encompassing a frequency range from 105 to 0.001 Hz.

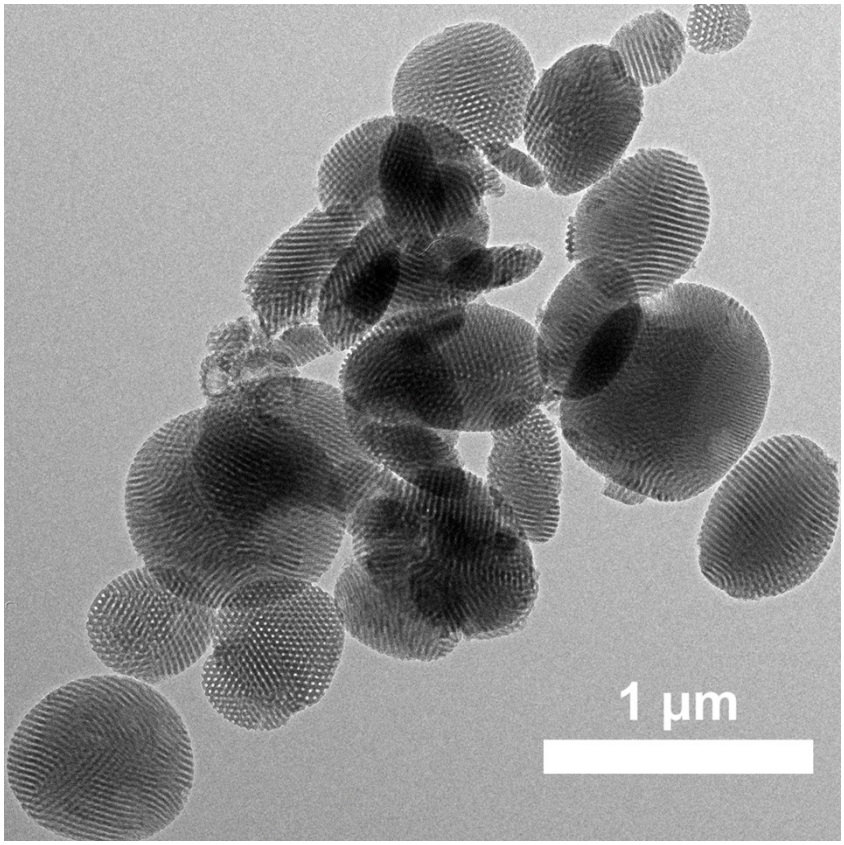

Figure S1. TEM image of Lens-NMC.

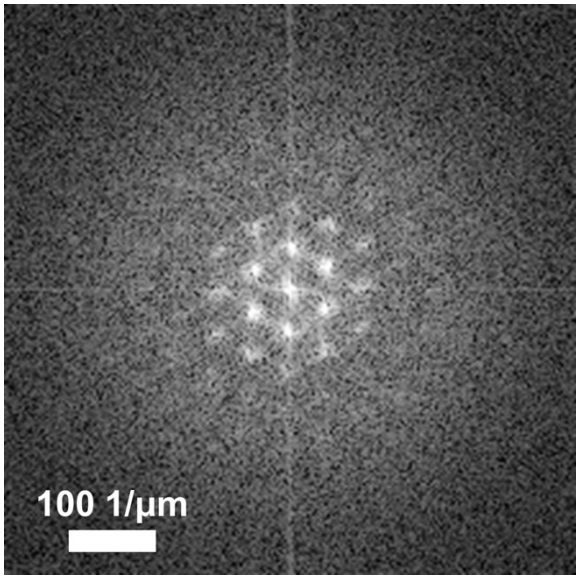

Figure S2. FFT diffractogram of Lens-NMC, obtained on parallel domain with pore axis**.**

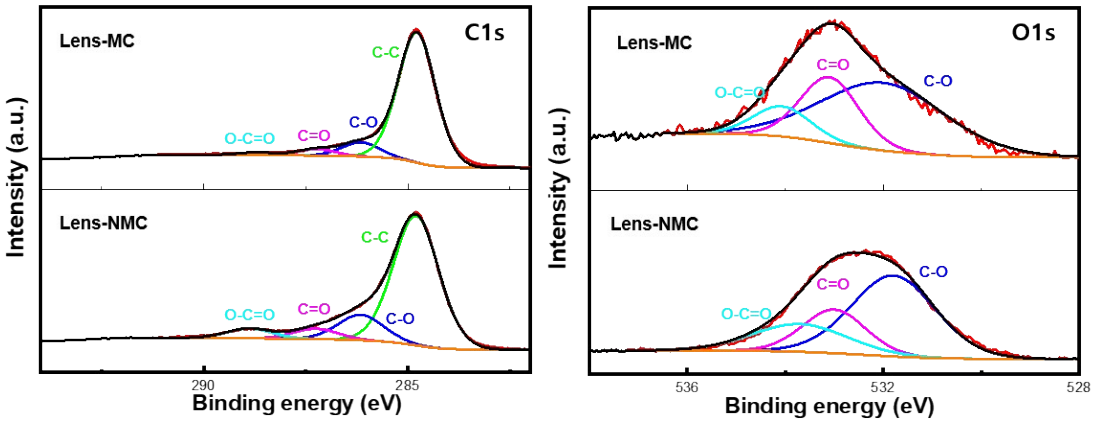

Figure S3. XPS C1s and O1s spectra of Lens-MC and Lens-NMC.

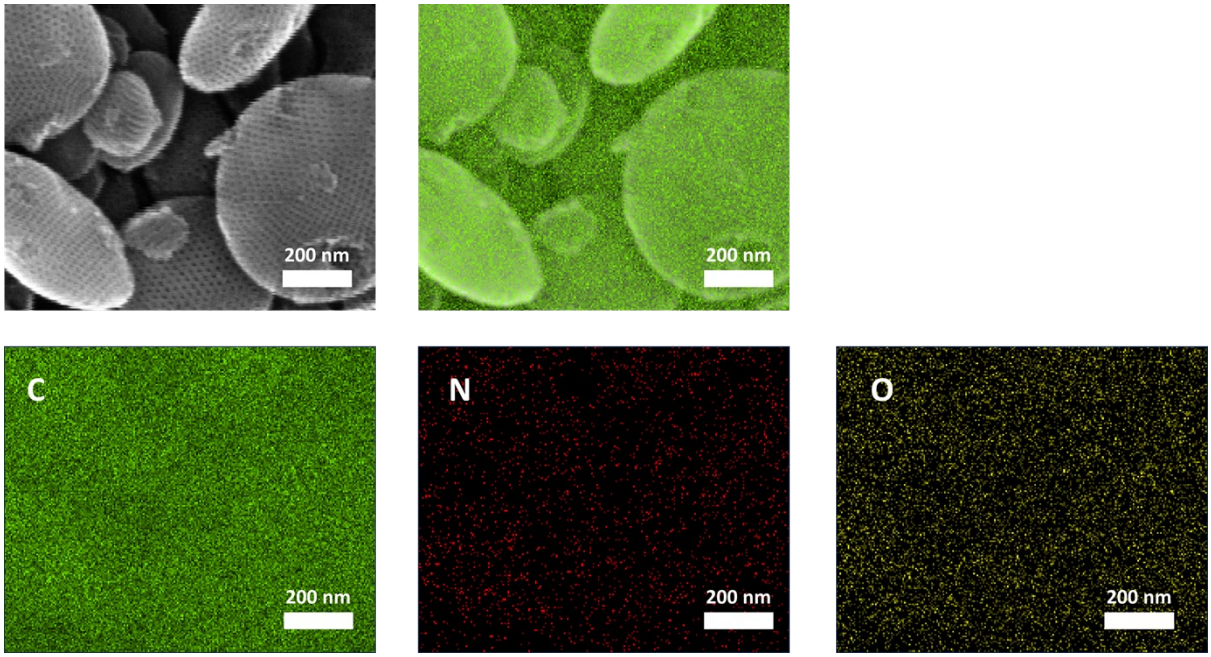

Figure S4. SEM images and corresponding EDX elemental mapping of Lens-NMC.

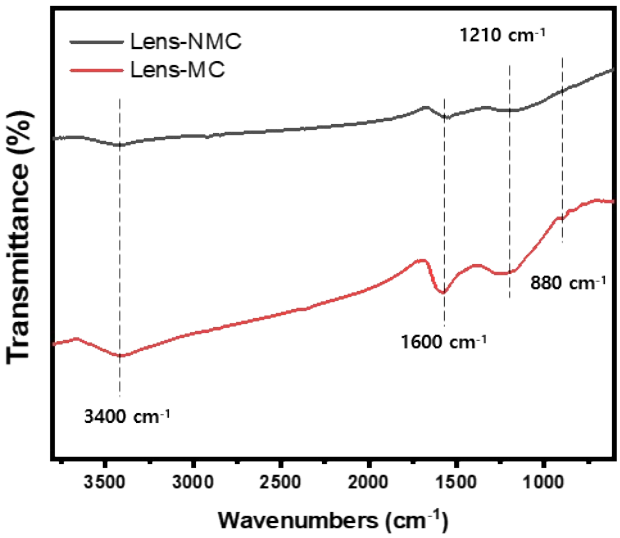

Figure S5. The FT-IR transmittance spectra of Lens-NMC and Lens-MC. A broad band around 3400 cm^{-1} can be attributed to the stretching vibration of -OH groups, particularly those originating from the phenolic -OH groups present in PF resin. The stretching vibration of aromatic C-C bonds are revealed around 1600 cm^{-1} while the stretching vibrations associated with the C-O bonds in the phenolic group are observed at approximately 1210 cm^{-1}. Furthermore, the benzene ring substitution was appeared at around 880 cm^{-1} in spectra.

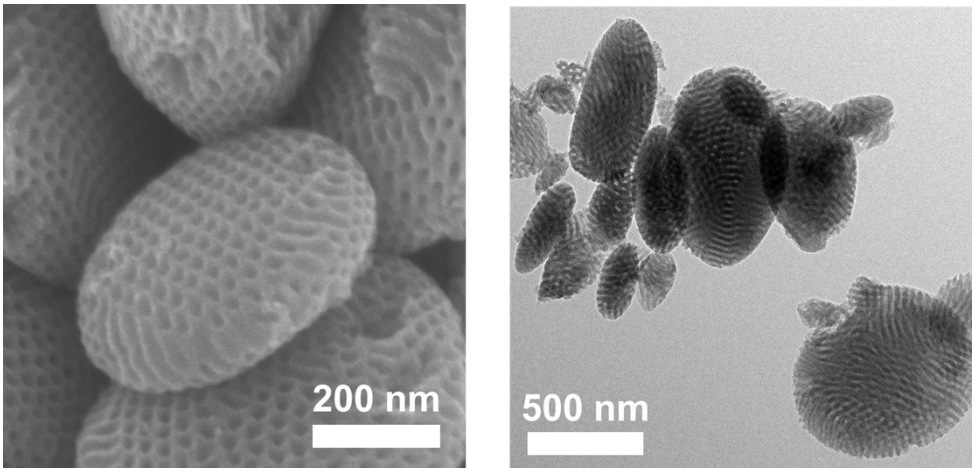

Figure S6. SEM (left) and TEM (right) image of Lens-MC.

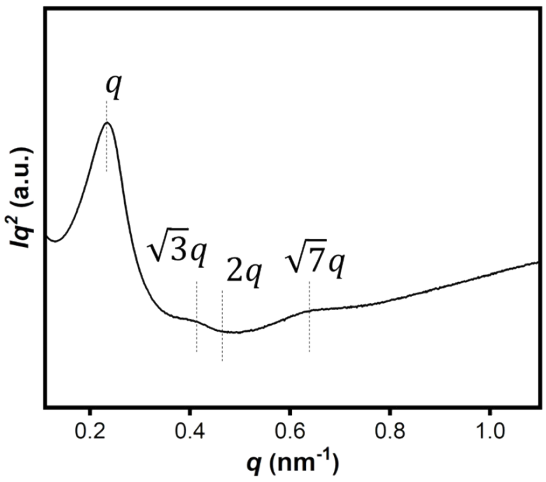

Figure S7. SAXS pattern of Lens-MC.

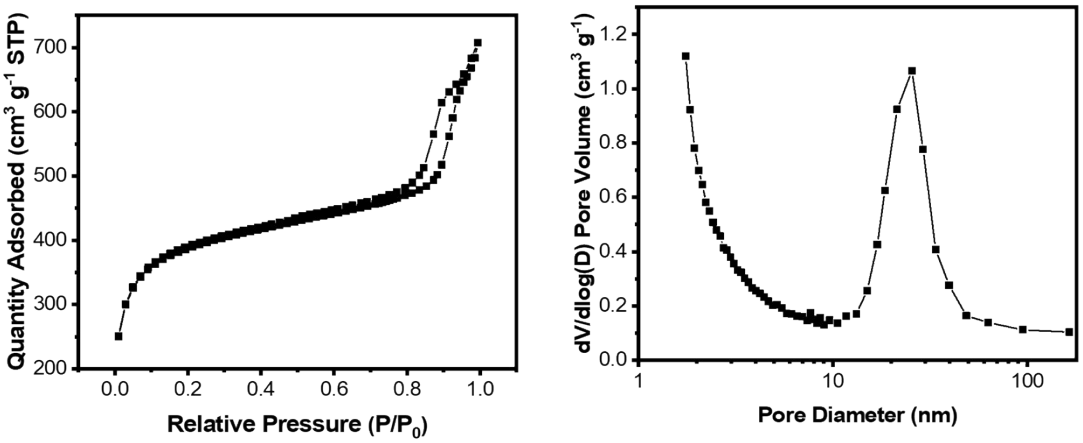

Figure S8. N_2 physisorption isotherm (left) and pore size distribution (right) of Lens-MC.

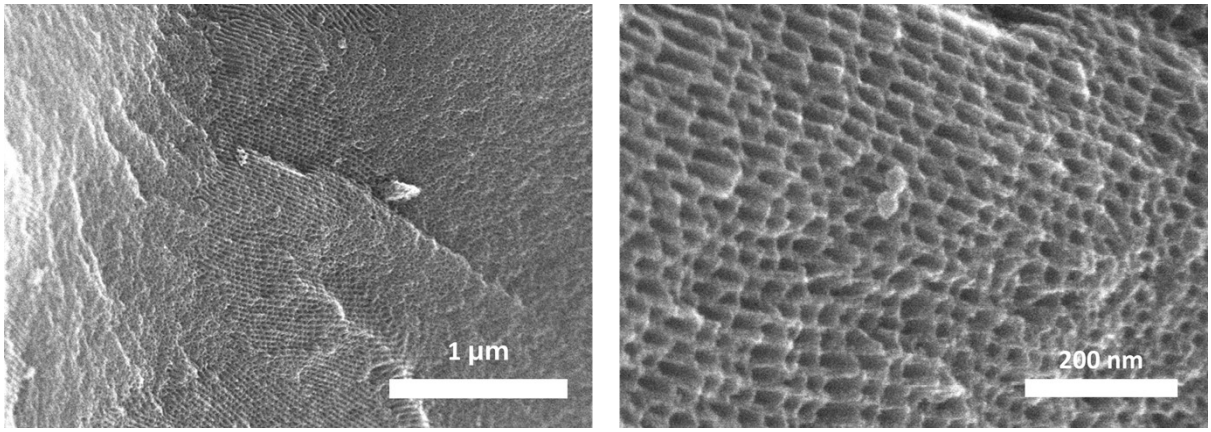

Figure S9. SEM images of BMC

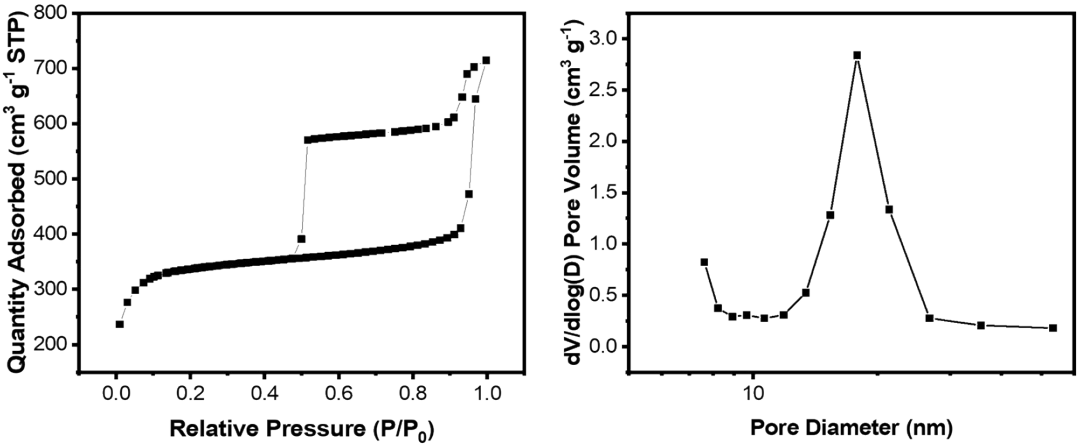

Figure S10. N_2 physisorption isotherm (left) and pore size distribution (right) of BMC

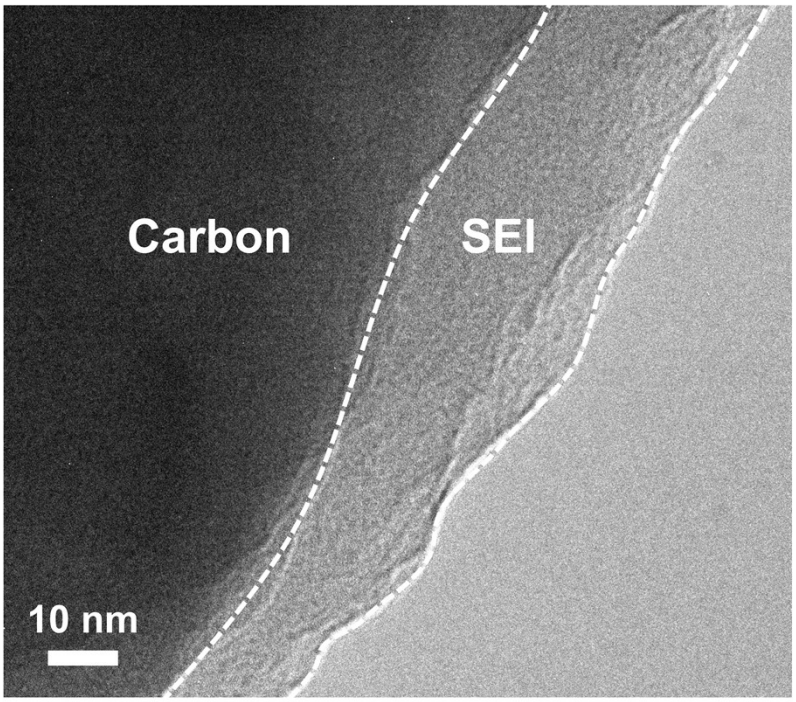

Figure S11. TEM images of Lens-NMC anode after first discharge to 0.01V.

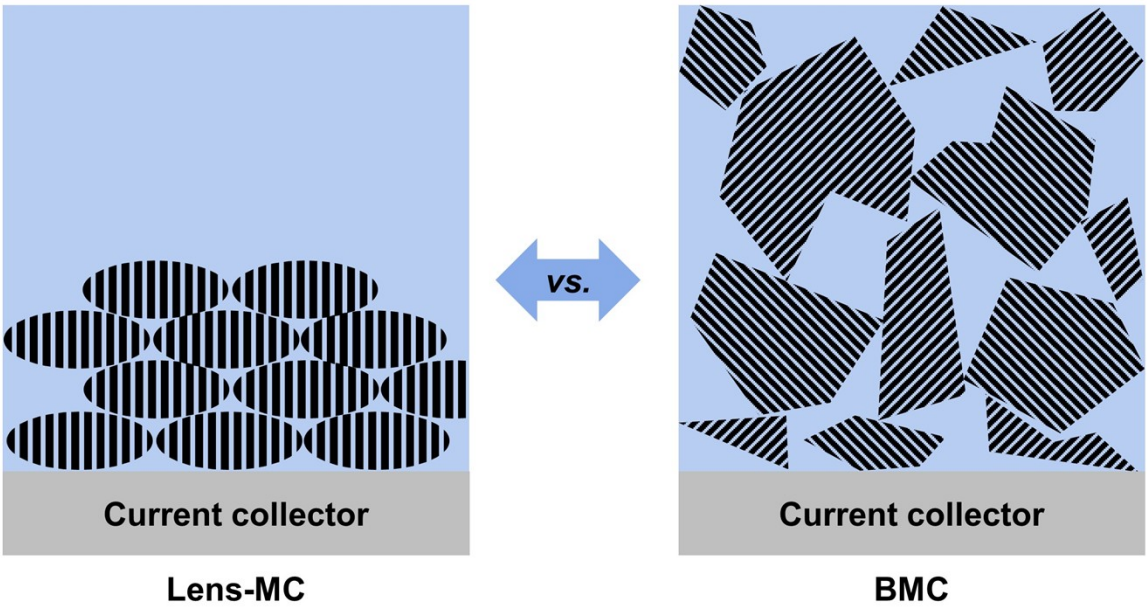

Figure S12. Schematic comparison of Lens-MC and BMC.

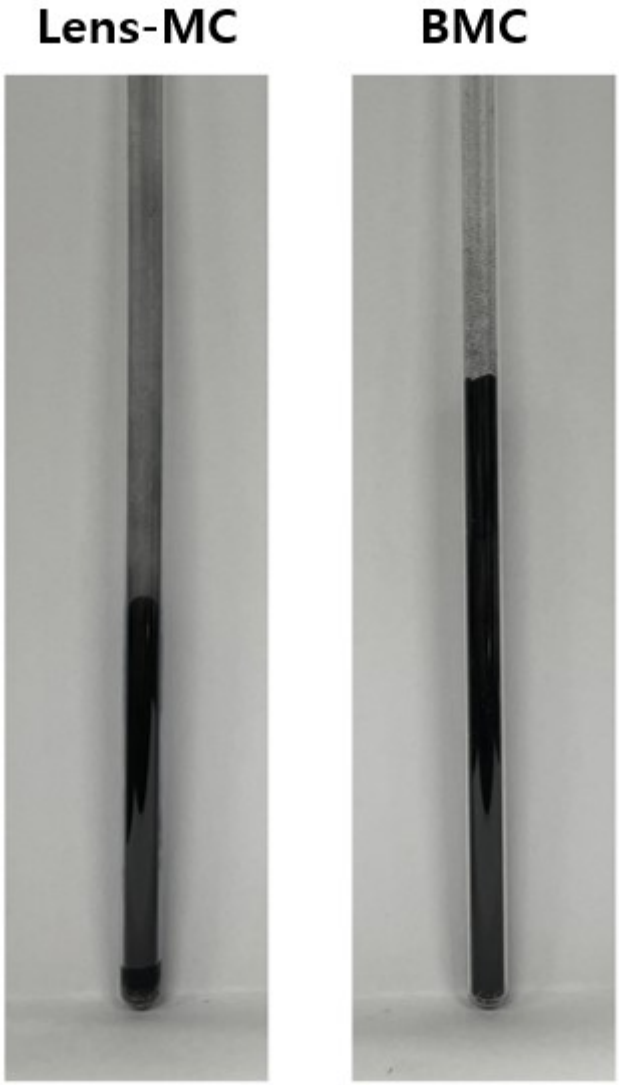

Figure S13. The comparison of tap densities of Lens-MC and BMC. 200 mg of each sample was filled in glass tubes with diameter of 5 mm.

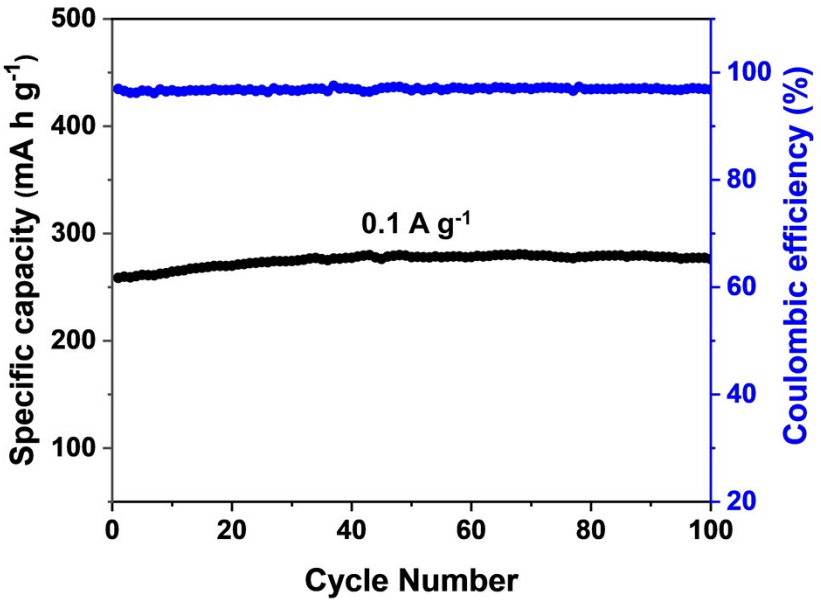

Figure S14. Cycling performance of Lens-NMC anode at 0.1 A g^{-1} over 100 cycles.

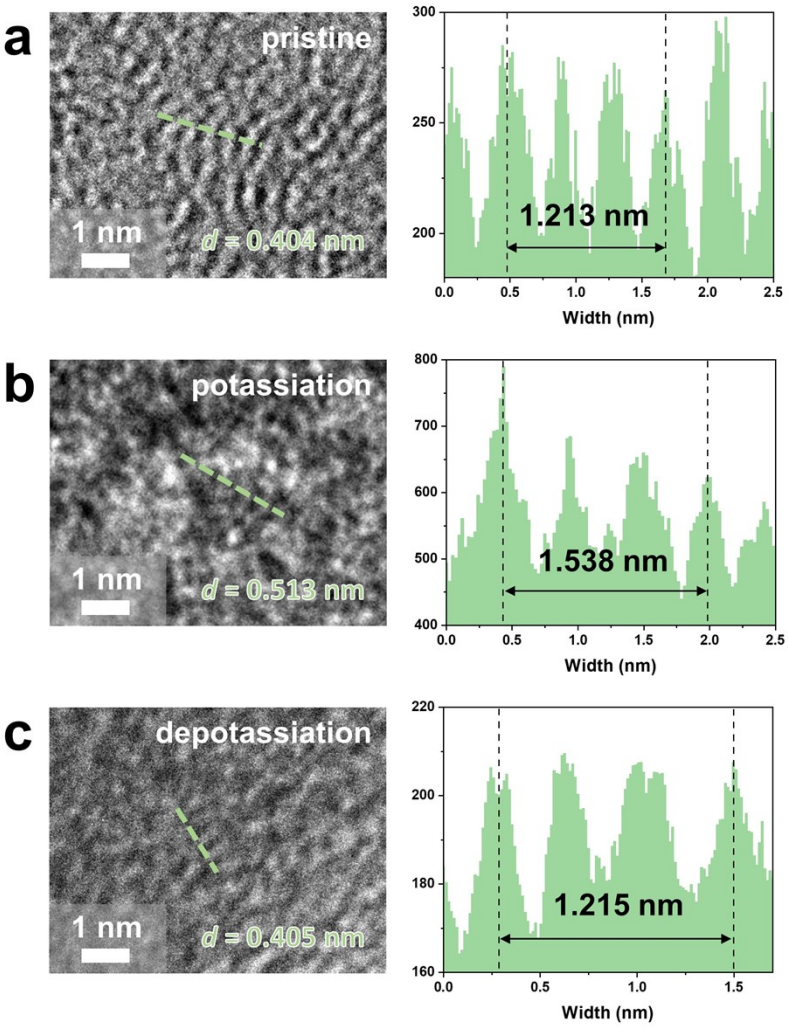

Figure S15. TEM images and corresponding interlayer spacing of (a) pristine, (b) potassiated, and (c) depotassiated Lens-NMC.

Table S1. Nitrogen physisorption isotherm analysis of Lens-NMC, Lens-MC and BMC.

Sample	**Surface area (m^2 g^{-1})**	**Pore volume (cm3 g^{-1})**	**Pore size (nm)**
Lens-NMC	1,367	1.20	25
Lens-MC	1,406	1.09	25
BMC	1,071	1.10	17

Table S2. Element analysis of Lens-NMC and Lens-MC.

Element (at%)	**Carbon**	**Hydrogen**	**Nitrogen**
Lens-NMC	86.3	2.08	2.92
Lens-MC	90.1	2.04	0.02

Table S3. Comparison of Lens-NMC electrode with reported carbonaceous anodes in KIBs at low and high current densities.

Anode material	Cyclability
Lens-NMC (this work)	276 mA h g^{-1}@0.1 A g^{-1} after 100 cycles 206 mA h g^{-1}@1 A g^{-1} after 2000 cycles
3D rGO aerogel[2]	230 mA h g^{-1}@0.093 A g^{-1} after 100 cycles 125 mA h g^{-1}@0.448 A g^{-1} after 500 cycles
N-doped necklace-like hollow carbon[3]	161 mA h g^{-1}@1 A g^{-1} after 1600 cycles
N-doped soft carbon[4]	165 mA h g^{-1}@1 A g^{-1} after 500 cycles
Pitch derived soft carbon[5]	278 mA h g^{-1}@0.028 A g^{-1} after 50 cycles 192 mA h g^{-1}@0.28 A g^{-1} after 1000 cycles
Hard carbon sphere[6]	264 mA h g^{-1}@0.02 A g^{-1} after 50 cycles
Oxygen functionalized hard carbon[7]	211.6 mA h g^{-1}@0.05 A g^{-1} after 200 cycles 90.2 mA h g^{-1}@4 A g^{-1} after 850 cycles
Vertically aligned Carbon aerogel[8]	151 mA h g^{-1}@0.14 A g^{-1} after 1000 cycles
P, N dual-doped hollow carbon sphere[9]	250.1 mA h g^{-1}@0.2 A g^{-1} after 500 cycles 141.2 mA h g^{-1}@1 A g^{-1} after 5000 cycles
Partially graphitic hard carbon[10]	200 mA h g^{-1}@0.1 A g^{-1} after 100 cycles
Porous carbon fiber[11]	259 mA h g^{-1}@0.05 A g^{-1} after 80 cycles 149 mA h g^{-1}@1 A g^{-1} after 3300 cycles

Table S4. The fitted parameters and values of the model for Lens-NMC and Lens-MC anode.

Anode	R_s (Ohm)	Q_1 ($F\ s^{-0.1686}$)	R_f (Ohm)	Q_2 ($F\ s^{-1}$)	R_{ct} (Ohm)	Z_w ($Ohm\ s^{-0.5}$)
Lens-NMC	2.123	32.5×10^{-6}	276.6	0.296×10^{-3}	0.6775	220
Lens-MC	2.391	25.07×10^{-6}	432.5	1.76×10^{-3}	2487	0.6688×10^{-27}

Reference

S1. S. Kim, M. Ju, J. Lee, J. Hwang and J. Lee, *J. Am. Chem. Soc.*, 2020, **142**, 9250-9257.

S2. L. Y. Liu, Z. F. Lin, J. Y. Chane-Ching, H. Shao, P. L. Taberna and P. Simon, *Energy Storage Mater.*, 2019, **19**, 306-313.

S3. W. X. Yang, J. H. Zhou, S. Wang, W. Y. Zhang, Z. C. Wang, F. Lv, K. Wang, Q. Sun and S. J. Guo, *Energy Environ. Sci.*, 2019, **12**, 1605-1612.

S4. C. Liu, N. Xiao, H. J. Li, Q. Dong, Y. W. Wang, H. Q. Li, S. F. Wang, X. Y. Zhang and J. S. Qiu, *Chem. Eng. J.*, 2020, **382**, 121759.

S5. Y. Liu, Y. X. Lu, Y. S. Xu, Q. S. Meng, J. C. Gao, Y. G. Sun, Y. S. Hu, B. B. Chang, C. T. Liu and A. M. Cao, *Adv. Mater.*, 2020, **32**, 2000505.

S6. J. Xu, C. Y. Fan, M. Y. Ou, S. X. Sun, Y. Xu, Y. Liu, X. Wang, Q. Li, C. Fang and J. T. Han, *Chem. Mater.*, 2022, **34**, 4202-4211.

S7. Z. Y. Liu, S. J. Wu, Y. Song, T. Yang, Z. H. Ma, X. D. Tian and Z. J. Liu, *ACS Appl. Mater. Interfaces,* 2022, **14**, 47674–47684.

S8. J. Wang, Z. Xu, J. C. Eloi, M. M. Titirici and S. J. Eichhorn, *Adv. Funct. Mater.,* 2022, **32**, 2110862.

S9. J. Y. Gao, G. R. Wang, W. T. Wang, L. Yu, B. Peng, A. El-Harairy, J. Li and G. Q. Zhang, *ACS Nano,* 2022, **16**, 6255-6265.

S10. L. Zhong, W. L. Zhang, S. R. Sun, L. Zhao, W. B. Jian, X. He, Z. Y. Xing, Z. X. Shi, Y. A. Chen, H. N. Alshareef and X. Q. Qiu, *Adv. Funct. Mater.,* 2023, **33**, 2211872.

S11. J. L. Sun, L. Ma, H. C. Sun, Y. H. Xu, J. L. Li, W. J. Mai and B. T. Liu, *Chem. Eng. J.,* 2023, **455**, 140902.